IOP Conf. Series: Earth and Environmental Science **162** (2018) 012012 doi:10.1088/1755-1315/162/1/012012

Numerical simulation of internal wave propagation over a variable topography

R K Yasmin and S R Pudjaprasetya

Department of Mathematics, Faculty of Mathematics and Natural Sciences, Institut Teknologi Bandung, Jalan Ganesha 10, Bandung, 40132, Indonesia

E-mail: rifadinaky@gmail.com, sr_pudjap@math.itb.ac.id

Abstract. The Boussinesq-type of equation is considered here as a model for describing interfacial wave dynamics in a two-layer fluid system. The equation, which is derived under rigid-lid assumption, has first order nonlinear term and dispersion term, and it holds for interfacial wave with long wavelength and small amplitude, relative to depth. The second-order Mac-Cormack scheme is implemented to solve this Boussinesq model. The numerical scheme is validated by simulating solitary wave as well as monotonic bore. Finally, the evolution of solitary wave propagating over a variable bathymetry with a shelf is examined.

1. Introduction

Internal wave are gravity wave that occur within ocean waters. Stratified ocean density support the existence of these internal wave. Typical ocean density is low near the surface and increases as depth increases. A layer of fluid with large density gradient is called a pycnocline. When pycnocline layer is relatively thin, ocean density can be well-described as a two-layer fluid system. In this case, internal wave propagate horizontally along the pycnocline and are called interfacial wave. Propagation of these interfacial wave is often described by the Boussinesq model. This model is a depth integrated two-layer model that incorporates weakly nonlinear and dispersive effects. In the model formulation, assumption of shallow water and rigid-lid approximation are applied.

Internal wave are ubiquitous. A comprehensive survey about this natural phenomena can be found for instance in Gerkema [1]. Several theoretical models have been derived to describe the dynamics of internal wave. To resemble the original situation in nature, Osborne and Burch [2], Liu [3], and Helfrich [4] observed the dissipation and shoaling effect of internal wave by using the Korteweg-de Vries (KdV) equation, whereas Holloway et al. [5] used the rotated-modified extended KdV equation. Duda et al. [6] used the extended KdV to study the behaviour of two kinds of internal wave: large amplitude solitary wave and internal tide. In the other hand, an experimental and numerical study of internal wave generation was conducted by Lin and Liu [7].

Tomasson and Melville [8], as well as Lynett and Liu [9], formulated a depth-integrated model to examine internal wave dynamics in a two-layer fluid. The Boussinesq-type equations were derived using the perturbation method of two small parameters representing the ratio of amplitude to depth and depth to wavelength. This high order Boussinesq model was then solved using the fourth-order predictor-corrector scheme. In this paper, the Boussinesq model of

Lynett and Liu [9] is adopted and restricted to one dimension model of first order term. Then, the finite difference Mac-Cormack method is implemented to solve these equations. Validation of the scheme is presented via two test cases: simulation of solitary wave propagation and monotonic bore. These test cases indicate that the proposed scheme can handle non-linearity and dispersion with good balance. Further, deformation of a solitary wave when it propagates over a shelf-topography is also presented.

2. Depth-averaged two-layer model

In this section, a direct derivation of one-dimensional Boussinesq equations will be discussed, starting from the full governing equation. Consider a fluid domain with a thin pycnocline layer, in such a way that it can be represented as a two-layer homogeneous fluid: the upper fluid layer with density ρ_1 and the lower fluid layer with density ρ_2, as illustrated in Figure 1.

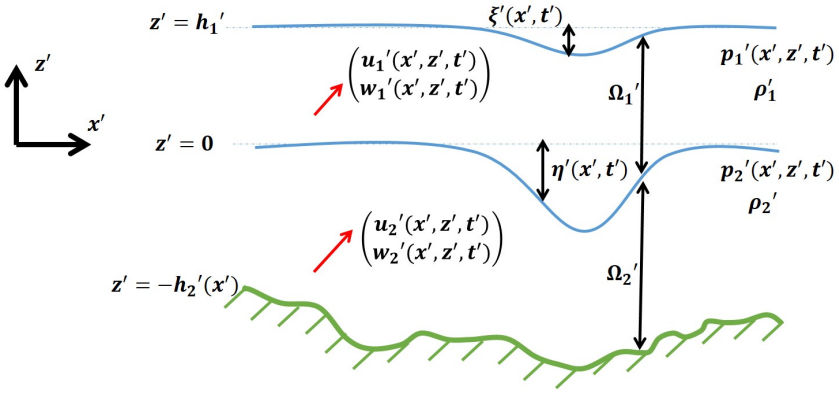

Figure 1. Sketch of a two-layer fluid system.

The undisturbed levels are: free surface $z = h_1$, interface $z = 0$, and bottom topography $z = -h_2(x)$. The interface displacement is denoted by η' and the free surface displacement is ξ', with a positive sign represents an upward displacement. The two-layer fluid domains are denoted as

$$\Omega_1' = \{(x', z') \mid \eta' < z' < \xi' + h_1', x' \in R\}, \text{ and}$$
$$\Omega_2' = \{(x', z') \mid -h_2' < z' < \eta', x' \in R\}.$$

Density, pressure, and particle velocities in the upper layer are respectively represented by ρ_1', p_1', and $\begin{pmatrix} u_1' \\ w_1' \end{pmatrix}$, whereas in the lower layer by ρ_2', p_2', and $\begin{pmatrix} u_2' \\ w_2' \end{pmatrix}$. Amplitude and wavelength of the internal wave are denoted by a_0 and l_0, respectively.

To formulate the depth averaged model for interfacial wave, the normalized variables are introduced first [9]. Let l_0 and h_0 be the horizontal and vertical length scales, respectively, $\frac{l_0}{\sqrt{g^* h_0}}$ be the time scale and a_0 be the scale of wave amplitude, therefore the non-dimensional variables will take form as follow

$$x = \frac{x'}{l_0}, \qquad z = \frac{z'}{h_0}, \qquad t = \frac{t'\sqrt{g^* h_0}}{l_0},$$

$$\eta = \frac{\eta'}{a_0}, \qquad \Delta\rho = \frac{\Delta\rho'}{\rho_0}, \qquad \xi = \frac{\xi'}{a_0 \Delta\rho},$$

$$(h_1, h_2) = \frac{(h_1', h_2')}{h_0}, \quad (p_1, p_2) = \frac{(p_1', p_2')}{\rho_0 g^* a_0}, \quad (\rho_1, \rho_2) = \frac{(\rho_1', \rho_2')}{\rho_0},$$

$$(u_1, u_2) = \frac{(u_1', u_2')}{\varepsilon\sqrt{g^* h_0}}, \quad (w_1, w_2) = \frac{(w_1', w_2')}{\frac{\varepsilon}{\mu}\sqrt{g^* h_0}},$$

where the parameters are

$$\rho_0 = \rho_2', \qquad g^* = g\frac{\Delta\rho'}{\rho_0}, \qquad h_0 = \frac{h_1' h_2'}{h_1' + h_2'}. \tag{1}$$

On those scalings, two small parameters were introduced as follow

$$\varepsilon = \frac{a_0}{h_0}, \quad \text{and} \quad \mu = \frac{h_0}{l_0}, \tag{2}$$

each represent nonlinearity and dispersion, respectively.

In dimensionless variables, the two-layer homogeneous fluid domains are Ω_1 and Ω_2, which represent the upper and lower layer, respectively. The Euler equations for each fluid domain are following

$$\mu^2 \frac{\partial u_j}{\partial x} + \frac{\partial w_j}{\partial z} = 0 \qquad \text{in } \Omega_j, \tag{3}$$

$$\frac{\partial u_j}{\partial t} + \varepsilon u_j \frac{\partial u_j}{\partial x} + \frac{\varepsilon}{\mu^2} w_j \frac{\partial u_j}{\partial z} = -\frac{1}{\rho_j}\frac{\partial p_j}{\partial x} \text{ in } \Omega_j, \tag{4}$$

$$\varepsilon\frac{\partial w_j}{\partial t} + \varepsilon^2 u_j \frac{\partial w_j}{\partial x} + \frac{\varepsilon^2}{\mu^2} w_j \frac{\partial w_j}{\partial z} = -\frac{\varepsilon}{\rho_j}\frac{\partial p_j}{\partial z} \text{ in } \Omega_j, \tag{5}$$

for $j = 1, 2$. In the above equations, indices $j = 1$ and $j = 2$ represent the upper and lower layer, respectively.

Furthermore, several boundary conditions are applied. Along the free surface ($z = h_1 + \varepsilon\xi\Delta\rho$) the total pressure vanishes

$$p_1 = \rho_1 \xi, \tag{6}$$

and the kinematic boundary condition along the surface reads

$$W = \mu^2 \Delta\rho(\xi_t + \varepsilon\xi_x U). \tag{7}$$

Meanwhile, along the interface ($z = \varepsilon\eta$), the pressure is continuous

$$p_2 = p_1 + \eta, \tag{8}$$

and the kinematic boundary condition read as

$$W = \mu^2(\eta_t + \varepsilon\eta_x U), \tag{9}$$

$$w = \mu^2(\eta_t + \varepsilon\eta_x u), \tag{10}$$

or it can be written

$$W - \mu^2 \varepsilon \eta_x U = w - \mu^2 \varepsilon \eta_x u.$$

Finally, along the bottom ($z = -h_2$), the impermeable boundary condition is applied

$$w = -\mu^2 h_{2_x} u. \tag{11}$$

To summarize, the governing equations for internal wave propagation in two-layer system fluids are equations (3)-(5), with boundary conditions (7)-(11).

Internal wave appears within the ocean body. Although there are internal wave with large amplitude within the ocean, the free surface above them is nearly undisturbed; only ripples may appears at the surface [3]. One common approach is assuming the free surface to be zero at all times, which is known as the rigid-lid assumption. Under the rigid-lid assumption, which is simply $\xi(x,t) = 0$, the upper fluid is $\varepsilon\eta(x,t) < z < h_1$, $x \in R$ and the lower layer fluid is $-h_2 < z < \varepsilon\eta$, $x \in R$.

Next, the depth averaged velocity for the upper layer and lower layer are defined as

$$\bar{u_1}(x,t) = \frac{1}{h_1 - \varepsilon\eta} \int_{\varepsilon\eta}^{h_1} u_1 dz, \tag{12}$$

$$\bar{u_2}(x,t) = \frac{1}{h_2 + \varepsilon\eta} \int_{-h_2}^{\varepsilon\eta} u_2 dz, \tag{13}$$

respectively. Later, the above depth averaged formulations together with boundary conditions will be used to derive the Boussinesq equations.

The following equation is obtained from the relation (13) and the lower layer boundary conditions

$$\begin{aligned} ((h_2 + \varepsilon\eta)\bar{u_2})_x &= \frac{\partial}{\partial x} \int_{-h_2}^{\varepsilon\eta} u_2 dz \\ \Leftrightarrow \qquad (h_2 + \varepsilon\eta)_x \bar{u_2} + (h_2 + \varepsilon\eta)\bar{u_2}_x &= \int_{-h_2}^{\varepsilon\eta} u_{2_x} dz + u_2|_{\varepsilon\eta} (\varepsilon\eta)_x + u_2|_{-h_2} h_{2_x}. \end{aligned}$$

Under the shallow water assumption, the horizontal velocity is homogeneous over the fluid depth, so $u_2(-h_2,t) = \bar{u_2}(x,t) = u_2(\varepsilon\eta,t)$, therefore the first term on the left hand side and the second and third terms on the right hand side are cancelled out. Hence

$$(h_2 + \varepsilon\eta)\bar{u_2}_x = \int_{-h_2}^{\varepsilon\eta} u_{2_x} dz.$$

Integrating the continuity equation for the lower layer (equation (3) for $j = 2$) over the depth from $z = -h_2$ to $z = \varepsilon\eta$ yields

$$\begin{aligned} \int_{-h_2}^{\varepsilon\eta} \left(\mu^2 \frac{\partial u_2}{\partial x} + \frac{\partial w_2}{\partial z} \right) dz &= 0 \\ \Leftrightarrow \qquad \mu^2 (h_2 + \varepsilon\eta)\bar{u_2}_x + w_2|_{\varepsilon\eta} - w_2|_{-h_2} &= 0 \\ \Leftrightarrow \qquad \eta_t + ((h_2 + \varepsilon\eta)\bar{u_2})_x &= 0. \end{aligned}$$

The last relation is obtained after adopting boundary conditions (10) and (11).

Performing the analogue process for the upper layer, and using boundary conditions (7) and (9) yield

$$\eta_t - ((h_1 - \varepsilon\eta)\bar{u_1})_x = 0.$$

Let M denotes fluid discharge from the lower layer to the upper layer. Mass conservation for each layer requires that M should be equal to the reverse discharge: from the upper layer to the lower layer, which is expressed as follows

$$(h_2 + \varepsilon\eta)\bar{u_2} = M = -(h_1 - \varepsilon\eta)\bar{u_1}, \tag{14}$$

Then, the continuity equation expressed in depth averaged variables is

$$\eta_t + M_x = 0.$$

For the momentum equation, by assuming that density difference between layers is small, i.e. $\mathcal{O}(\mu^4)$, the equation can be obtained by means of perturbation method [9]. The resulting equation contains terms of successive order $\mathcal{O}(1)$, $\mathcal{O}(\varepsilon)$, $\mathcal{O}(\varepsilon^2)$, $\cdots$, as well as terms of $\mathcal{O}(\mu^2)$, $\mathcal{O}(\mu^4)$, $\cdots$. Keeping terms up to $\mathcal{O}(\varepsilon), \mathcal{O}(\mu^2)$, and neglecting higher order terms, the depth averaged model for interfacial wave are following

$$\eta_t + M_x = 0 \tag{15}$$

$$\begin{aligned} &M_t + a\eta_x + b\left(MM_x - (M\eta)_t\right) + cM^2 h_{2_x} \\ &+d\left((M\eta^2)_t - M(M\eta)_x - \eta M M_x\right) + eM_{xxt} \\ &+f\left(M_{xt}h_{2_x} - \frac{2}{h_2}M_t h_{2_x}^2 + (M_t h_{2_x})_x\right) = 0 \end{aligned} \tag{16}$$

where

$$a = \left(\frac{1}{h_1} + \frac{1}{h_2}\right)^{-1}, \qquad b = \varepsilon\left(\frac{1}{h_1} - \frac{1}{h_2}\right), \qquad c = -\varepsilon\frac{1}{h_1^3}a,$$
$$d = \varepsilon^2\left(\frac{1}{h_1^2} - \frac{1}{h_1 h_2} + \frac{1}{h_2^2}\right), \qquad e = \mu^2\frac{h_1 h_2}{3}, \qquad f = -\mu^2 a.$$

In further discussions, equations (15, 16) will be solved numerically. Then, various simulations will be presented under Boussinesq assumption, i.e. the non-linearity and the dispersion are in the same order $\mathcal{O}(\varepsilon) = \mathcal{O}(\mu^2)$.

3. Mac-Cormack method

In this section a numerical scheme to solve the equations (15, 16) is formulated. Here the Mac-Cormack scheme is implemented, which is a suitable scheme for solving hyperbolic problems [10]. The Mac-Cormack method is a finite difference second-order predictor-corrector scheme. Firstly, note that the equation (16) contains term with mixed derivative. To handle this situation, a new variable φ is introduced as follows

$$\varphi = M - bM\eta + dM\eta^2 + eM_{xx} + f\left(2h_{2_x}M_x - \frac{2}{h_2}h_{2_x}^2 M + h_{2_{xx}}M\right).$$

Written in the new variable φ, equation (16) becomes

$$\varphi_t + \left(a - dM^2\right)\eta_x + (b - 2d\eta)\,MM_x + cM^2 h_{2_x} = 0.$$

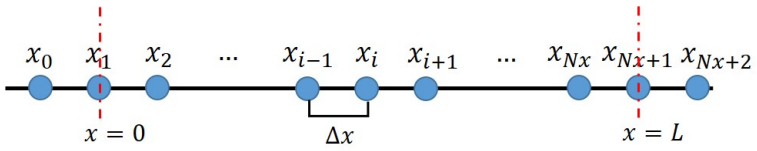

Figure 2. Space domain discretization.

Let Δt be the length of time step, and discrete time variable is denoted as $t_n = (n-1)\Delta t$, $n = 1, 2, \cdots, Nt+1$, whereas Δx is the length of space step, and discrete space variable is denoted as $x_i = (i-1)\Delta x$, $i = 1, 2, \cdots, Nx+1$, in the computational domain $[0, L]$, see Figure 2. Notation η_j^n represents the value of η at space grid j and time grid n, so do φ_j^n and M_j^n.

The predictor step is a forward-time forward-space approximation,

$$\overline{\eta_i^{n+1}} = \eta_i^n - \frac{\Delta t}{\Delta x}\left(M_{i+1}^n - M_i^n\right) \tag{17}$$

$$\begin{aligned}\overline{\varphi_i^{n+1}} = \varphi_i^n &- \frac{\left(a_i - d_i(M_i^n)^2\right)\Delta t}{\Delta x}\left(\eta_{i+1}^n - \eta_i^n\right) - \frac{c_i \Delta t}{\Delta x}(M_i^n)^2 h_{2_{x_i}} \\ &- \frac{\left(b_i - 2d_i\eta_i^n\right)\Delta t}{\Delta x} M_i^n \left(M_{i+1}^n - M_i^n\right).\end{aligned} \tag{18}$$

The overlines indicate predicted values. In the end of each time-step, the predicted values $\overline{M_i^{n+1}}$ for $i = 2, 3, \ldots, Nx$ can be obtained by solving $\overline{D}\,\overline{M^{n+1}} = \overline{\varphi^{n+1}}$, where

$$\overline{D} = \overline{g^*} + k^* + \frac{1}{\Delta x^2} e^*, \tag{19}$$

$$\overline{g^*} = \begin{pmatrix} \overline{g_2} & 0 & \cdots & 0 \\ 0 & \overline{g_3} & \cdots & 0 \\ \vdots & \vdots & \ddots & \vdots \\ 0 & \cdots & 0 & \overline{g_{Nx}} \end{pmatrix}, \qquad k^* = \begin{pmatrix} -k_2 & k_2 & 0 & \cdots & 0 \\ 0 & -k_3 & k_3 & \cdots & 0 \\ \vdots & \vdots & \ddots & \vdots & \vdots \\ 0 & \cdots & 0 & -k_{Nx-1} & k_{Nx-1} \\ 0 & \cdots & 0 & 0 & -k_{Nx} \end{pmatrix},$$

$$e^* = \begin{pmatrix} -2e_2 & e_2 & 0 & \cdots & 0 \\ e_3 & -2e_3 & e_3 & \cdots & 0 \\ \vdots & \vdots & \ddots & \vdots & \vdots \\ 0 & \cdots & e_{Nx-1} & -2e_{Nx-1} & e_{Nx-1} \\ 0 & \cdots & 0 & e_{Nx} & -2e_{Nx} \end{pmatrix},$$

$$\overline{g_i} = 1 - b_i\overline{\eta_i^{n+1}} + d_i\overline{\eta_i^{n+1}}\ \overline{\eta_i^{n+1}} - \frac{2f_i}{h_2}h_{2_{x_i}}^2 + f_i h_{2_{xx_i}}, \text{ and}$$

$$k_i = 2f_i h_{2_{x_i}}.$$

Meanwhile, the corrector step is the forward-time scheme with the average between the backward-space of predicted-values at time $n+1$ and the forward-space of real-values at time

n,

$$\eta_i^{n+1} = \eta_i^n - \frac{\Delta t}{2\Delta x}\left[\left(M_{i+1}^n - M_i^n\right) + \left(\overline{M_i^{n+1}} - \overline{M_{i-1}^{n+1}}\right)\right] \tag{20}$$

$$\begin{aligned}\varphi_i^{n+1} = \varphi_i^n &- \frac{\left(a_i - d_i(M_i^n)^2\right)\Delta t}{2\Delta x}\left[\left(\eta_{i+1}^n - \eta_i^n\right) + \left(\overline{\eta_i^{n+1}} - \overline{\eta_{i-1}^{n+1}}\right)\right] \\ &- \frac{\left(b_i - 2d_i\eta_i^n\right)\Delta t}{2\Delta x} M_i^n \left[\left(M_{i+1}^n - M_i^n\right) + \left(\overline{M_i^{n+1}} - \overline{M_{i-1}^{n+1}}\right)\right] \\ &- \frac{c_i \Delta t}{\Delta x}(M_i^n)^2 h_{2_{x_i}}.\end{aligned} \tag{21}$$

The values of M_i^{n+1} for $i = 2, 3, \ldots, Nx$ can be obtained in the end of each time-step by solving $DM^{n+1} = \varphi^{n+1}$, where

$$D = g^* + k^* + \frac{1}{\Delta x^2} e^*, \tag{22}$$

$$g^* = \begin{pmatrix} g_2 & 0 & \cdots & 0 \\ 0 & g_3 & \cdots & 0 \\ \vdots & \vdots & \ddots & \vdots \\ 0 & \cdots & 0 & g_{Nx} \end{pmatrix}, \text{ and}$$

$$g_i = 1 - b_i\eta_i^{n+1} + d_i\eta_i^{n+1}\eta_i^{n+1} - \frac{2f_i}{h_2} h_{2_{x_i}}^2 + f_i h_{2_{xx_i}}.$$

Stencil of the numerical scheme above is illustrated in Figure 3. Note that both left and right boundary condition is needed to perform this numerical scheme.

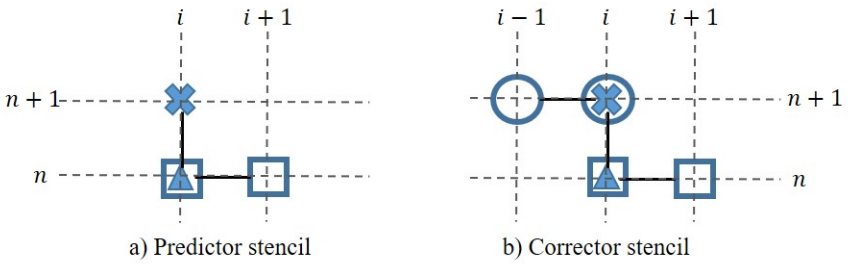

Figure 3. Stencil of Mac-Cormack Method.

4. Numerical simulation

To run the numerical simulation, as mentioned earlier, a left and right boundary condition is needed. In this paper, hard-wall boundary conditions are adopted for both ends, written as follow

$$\begin{aligned} \bar{u_1}(0,t) &= 0 \qquad \text{and} \qquad \bar{u_1}(L,t) = 0, \\ \bar{u_2}(0,t) &= 0 \qquad \text{and} \qquad \bar{u_2}(L,t) = 0, \end{aligned}$$

for $t > 0$. Since $(h_2 + \varepsilon\eta)\bar{u_2} = M = -(h_1 - \varepsilon\eta)\bar{u_1}$, the hard-wall boundary conditions imply

$$M(0,t) = 0 \qquad \text{and} \qquad M(L,t) = 0, \qquad \forall t > 0 \tag{23}$$

or in the discretized domain can be written as

$$M_1^n = 0 \qquad \text{and} \qquad M_{Nx+1}^n = 0, \qquad n = 1, 2, \cdots, Nt.$$

Afterwards, apply the Lax-Wendroff method to the continuity equation at both end of the space domain to get the boundary condition for η

$$\eta_1^{n+1} = \eta_1^n - \frac{\Delta t}{2\Delta x}\left(M_2^n - M_1^n\right) + \frac{1}{2}\left(\frac{\Delta t}{\Delta x}\right)^2 \left(M_2^n - 2M_1^n + M_0^n\right) \tag{24}$$

$$\begin{aligned}\eta_{Nx+1}^{n+1} = \eta_{Nx+1}^n &- \frac{\Delta t}{2\Delta x}\left(M_{Nx+2}^n - M_{Nx+1}^n\right) \\ &+ \frac{1}{2}\left(\frac{\Delta t}{\Delta x}\right)^2 \left(M_{Nx+2}^n - 2M_{Nx+1}^n + M_{Nx}^n\right).\end{aligned} \tag{25}$$

As illustrated in Figure 2, the point x_0 and x_{Nx+2} are outside the calculation domain. From (23), the value of M_0 can be obtained as an odd function interpolated from M_1 and M_2, or to be explicit $M_0 = -M_2$. And the same thing holds for M_{Nx+2}. With these results, equations (24, 25) can be written as

$$\eta_1^{n+1} = \eta_1^n - \frac{\Delta t}{2\Delta x} M_2^n$$
$$\eta_{Nx+1}^{n+1} = \eta_{Nx+1}^n + \frac{\Delta t}{2\Delta x} M_{Nx}^n,$$

which are the boundary conditions for η as a result from the hard-wall boundary condition.

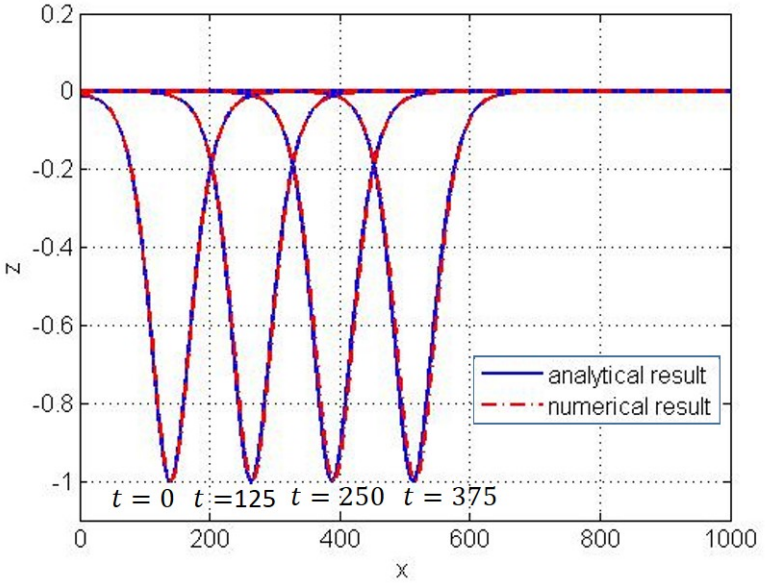

Figure 4. Solitary wave simulation using $\varepsilon = \mu^2 = 0.01$.

The numerical simulations will be conducted under Boussinesq assumption $O(\varepsilon) = O(\mu^2)$. Moreover, the higher terms such as $O(\varepsilon^2)$, $O(\varepsilon\mu)$, $O(\mu^3)$, etc. will be omitted. The first test case is performed to check whether the numerical solution is consistent to the known analytical

solution at constant depth. Two known analytical solutions are used for this test, a solitary wave and a monotonic bore.

The solitary wave has a dimensionless form as follows

$$\eta(x,t) = \mathrm{sech}^2\left(\frac{x-mt}{l}\right), \tag{26}$$

where $m = 1 + \dfrac{\varepsilon(h_2-h_1)}{2h_1h_2}$ and $l = \dfrac{2h_1h_2}{\sqrt{3\varepsilon(h_2-h_1)}}$. A solitary wave with small nonlinearity, $\varepsilon = 0.01$, will be observed first. This simulation uses a constant depth $h_2 = 3$ and the ratio of the upper and lower layer depth $\dfrac{h_2}{h_1} = 2$. The domain is discretized by $\Delta x = 1$ and $\Delta t = 0.01$.

The analytic and numerical result are plotted simultaneously as it can be seen in Figure 4. The figure shows that the numerical calculation is stable and consistent to its analytical solution for a quite long time.

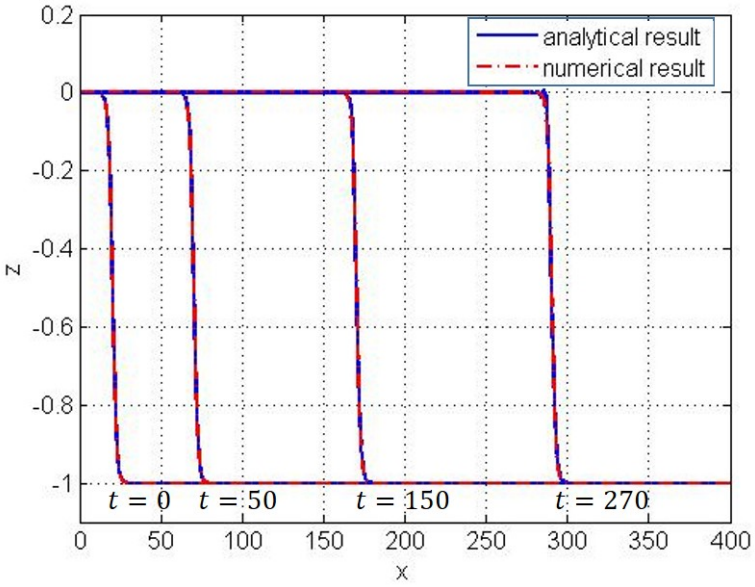

Figure 5. Monotonic bore simulation using $\varepsilon = \mu^2 = 0.01$.

A monotonic bore has the following dimensionless form

$$\eta(x,t) = \frac{1}{2}\left[1 + \tanh\left(\frac{x-mt}{l}\right)\right], \tag{27}$$

where $m = 1 + \dfrac{\left(h_2^2-h_1^2\right)^2}{8\left(h_2^3+h_1^3\right)}$ and $l = \sqrt{\dfrac{16\mu^2\left(h_2+h_1\right)\left(h_2^3+h_1^3\right)}{3\left(h_2^2-h_1^2\right)^2}}$. The simulation is conducted on a constant depth $h_2(x) = 2.1$ with the ratio between the upper and lower layers as $\dfrac{h_2}{h_1} = 1.1$. First, the simulation is performed for $\varepsilon = \mu^2 = 0.01$ using $\Delta x = 0.25$ and $\Delta t = 0.01$. The numerical result is stable and consistent to its analytical solution for eleven wavelengths of propagation as shown in Figure 5.

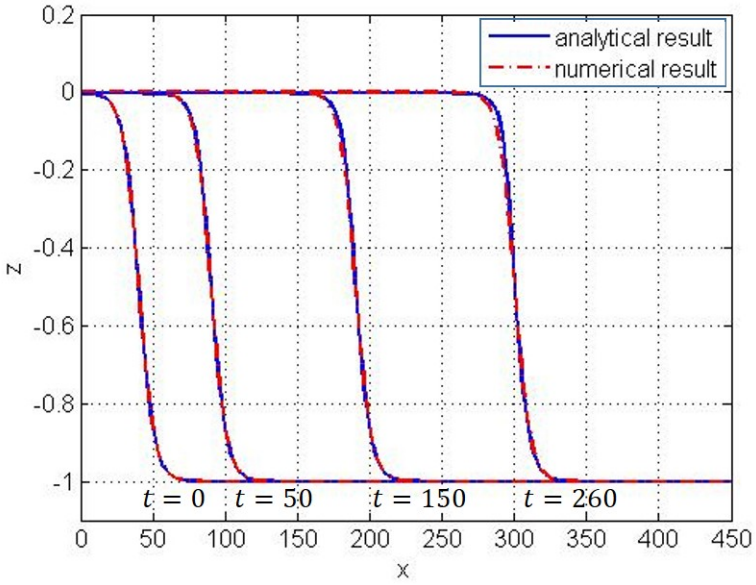

Figure 6. Monotonic bore using $\varepsilon = \mu^2 = 0.2$.

The second simulation is using larger parameter of nonlinearity, $\varepsilon = 0.2$. It was conducted using $\Delta x = 1.2$ and $\Delta t = 0.01$, and yields result in Figure 6. Again, it is shown that the simulated monotonic bore is in good agreement with the analytical bore.

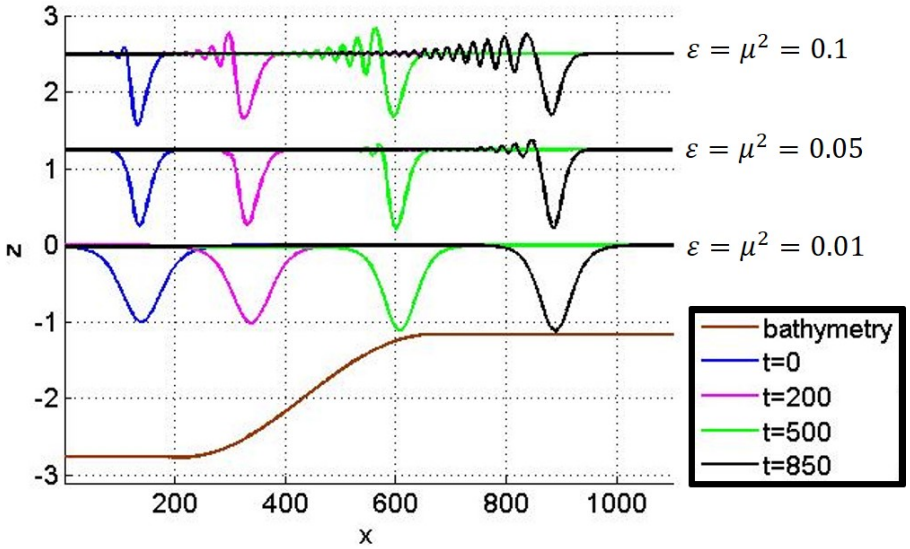

Figure 7. Simulation of a solitary wave evolving a shelf using $\varepsilon = \mu^2 = 0.1$, $\varepsilon = \mu^2 = 0.05$, and $\varepsilon = \mu^2 = 0.01$.

On the next test case, the behavior of a solitary wave that propagates over a shallower region

will be examined, which is expected to give a shoaling effect. Here we take a topography which has a smooth transition that connects two constant depths (calculated from the interface level): 100 m and 40 m [11]. The interface is located on 60 m under the sea level. Dimensionless parameters correspond to the above physical setting are $h_1 = \frac{8}{5}$, with the shelf topography is

$$h_{2o} + \frac{1}{2}\left(h_{2o} - h_{2e}\right)\left(\cos\left(\frac{\pi x}{L}\right) - 1\right),$$

where the upstream and downstream depths are $h_{2o} = \frac{8}{3}$ and $h_{2f} = \frac{16}{15}$, respectively. Simulations are conducted using several values of $\varepsilon = \mu^2$, i.e. 0.01, 0.05 and 0.1, and the results are plotted in Figure 7. For the case of $\mu = \varepsilon^2 = 0.01$, which is a small number, the initial solitary wave undergo the shoaling process which is almost linear. Simulation results of larger parameters $\mu = \varepsilon^2$ clearly demonstrate the effect of nonlinearity and dispersion; as the wave get steeper by nonlinearity, wave train appears due to dispersion, and hence the solitary wave develops into a negative leading wave followed by a wave train. Even though here the first order Boussinesq model is adopted, and solved using second-order Mac-Cormack method, the results are in good agreement with Lynett and Liu [9].

5. Conclusion

The implementation of Mac-Cormack method to the Boussinesq equations gave us a stable scheme. The scheme was validated by simulating the solitary wave solution that propagates undisturbed in shape with constant velocity. This solitary wave conform the analytical solitary wave. Another benchmark test was simulating the propagation of a monotonic bore. Simulations results demonstrated that the scheme can handle non-linearity and dispersion with good balance. Simulation of a solitary wave propagates over a topography with shelf displayed the shoaling phenomena. For a solitary wave with somewhat large non-linearity ε and dispersion μ^2 parameters, the wave undergo shoaling and dispersion effects, and the wave breaks down into a series of wave.

Acknowledgments

The authors acknowledge the financial support from Riset KK ITB 2017.

References

[1] Gerkema T and Zimmerman J T F 2008 *An Introduction to Internal Waves*(Texel : Royal NIOZ)
[2] Osborne A R and Burch T L 1980 Internal solitons in the andaman sea *Sci.* **208** 451-9
[3] Liu A K 1988 Analysis of nonlinear internal waves in New York Bight *J. Geophys. Res.* **93(C10)** 12317-29
[4] Helfrich K R 1992 Internal solitary wave breaking and run-up on a uniform slope *J. Fluid Mech.* **243** 133-54
[5] Holloway P E, Pelinovsky E and Talipova T 1999 A generalized Korteweg-de Vries model of internal tide transformation in the coastal zone *J. Geophys. Res.* **104(C8)** 18333-50
[6] Duda T F, Lynch J F, Irish J D, Beardsley R C, Ramp S R, Chiu C S, Tang T Y and Yang Y J 2004 Internal tide and nonlinear internal wave behavior at the continental slope in the northern south china sea *IEEE J. Oc. Engrg.* **29(4)** 1105-30
[7] Lin P and Liu P L F 1999 Internal wave-maker for Navier Stokes equations models *J. Wtrwy, Port, Coast., and Oc. Engrg.* **ASCE 125(4)** 207-16
[8] Tomasson G G and Melville W K 1992 Geostrophic adjustment in a channel : nonlinear and dispersive effects *J. Fluid Mech.* **241** 23-57
[9] Lynett P J and Liu P L F 2002 A two-dimensional, depth-integrated model for internal wave propagation over variable bathymatry *Wave Motion* **36** 221-40
[10] Garcia R and Kahawita R A 1986 Numerical solution of the St.Venant equations with the MacCormack finite-difference scheme *Int. J. Num. Methods in Fluids* **6** 259-74
[11] Liu A K, Chang Y S, Hsu M K and Liang N K 1998 Evolution of nonlinear internal waves in the East and South China Seas *J. Geophys. Res.* **103(C4)** 7995-8008